JOURNAL OF SOLID STATE CHEMISTRY **129,** 328–333 (1997)
ARTICLE NO. SC967260

Synthesis, Crystal Structure, and Magnetic Properties of a New Polymorphic Sodium Cobalt Phosphate with Trigonal Bipyramidal Co^{2+} and a Tunnel Structure

Pingyun Feng, Xianhui Bu, and Galen D. Stucky

Chemistry Department, University of California at Santa Barbara, Santa Barbara, California 93106

Received August 16, 1996; in revised form December 2, 1996; accepted December 9, 1996

A new sodium cobalt phosphate with a three-dimensional framework structure has been prepared by hydrothermal methods and characterized by single crystal X-ray diffraction and magnetic susceptibility measurements. The framework can be described as interconnected identical layers stacked along the crystallographic *a*-axis. The layer is built from half of the Co^{2+} trigonal bipyramids and half of the P^{5+} tetrahedra and can be classified as a distorted (4.8^2) net commonly found in zeolite frameworks. The structure has one-dimensional channels where charge-balancing sodium cations are situated. The Co–O–Co linkages give rise to a tetramer of Co^{2+} bipyramids which may be related to the low-temperature magnetic behavior. The magnetic susceptibility measurements show that the compound displays Curie–Weiss behavior down to a temperature of 15 K at which an antiferromagnetic phase transition occurs. The structural features and magnetic properties are compared with two other polymorphs of sodium cobalt phosphates which are built from tetrahedral and octahedral Co^{2+}, respectively. Crystal data for $NaCoPO_4$: $M = 176.89$, space group $P2_1/c$ (No. 14), $a = 5.7856(1)$, $b = 11.0954(2)$, $c = 9.9228(3)$, $\beta = 92.668(2)$, $V = 636.29(2)$ Å^3, $Z = 8$, $D_c = 3.693$ g cm^{-3}, dark red needle, Mo$K\alpha$, $\lambda = 0.71073$ Å, $\mu = 5.867$ mm^{-1}, $2\theta_{max} = 56.54°$, $R(F) = 2.07\%$ for 128 parameters and 1471 reflections with $I > 2\sigma(I)$.

INTRODUCTION

Framework structures containing metal or metalloid cations in various coordination polyhedra have been extensively studied. In oxide based materials, one of the most common coordinations encountered for metal or metalloid cations is tetrahedral, and these framework cations are referred to as "T" atoms. For example, zeolites usually consist of two different tetrahedral atoms such as Al^{3+} and Si^{4+} and can be referred to as tetrahedral–tetrahedral frameworks (1). Two other common framework types are tetrahedral–octahedral and octahedral–octahedral frameworks. To have large pores or channels, however, framework structures with octahedral centers are usually interrupted such as in cacoxenite (a mineral iron phosphate) and pharmacosiderite-type frameworks (2, 3). Some framework oxides also consist of metal or metalloid cations in trigonal coordinations. Examples include $Na_2Zn_3(CO_3)_4 \cdot 3H_2O$ (4), some borates such as $Zn_4O(BO_3)_2$ (5), and some tin(II) phosphates such as $Sn_3(PO_4)_2$ (6).

In comparison, oxide frameworks based on only tetrahedral and penta-coordinate metal or metalloid centers with no framework interruption are less common. Three examples are $FeAsO_4$ (7) with penta-coordinate Fe^{3+} connected by AsO_4 tetrahedra, Fe_3PO_7 (8) with penta-coordinate Fe^{3+} connected by PO_4 tetrahedra, and β-$Zn_3(PO_4)_2$ (9) with penta-coordinate Zn^{2+} joined by ZnO_4 and PO_4 tetrahedra. While there are many framework materials which consist of tetrahedral and penta-coordinate metal or metalloid centers, in most cases, these materials either contain additional metal or metalloid centers in other polyhedral configurations (most often octahedral, such as in $Fe_4(PO_4)_2O$ (10) and $AgCoPO_4$ (11) or at least one of five oxygen atoms (some may exist as hydroxyl groups or water molecules) coordinated to penta-coordinate metals are non bridging. Five-coordinate Al^{3+} and Ga^{3+} cations in as-synthesized open framework aluminophosphates and gallophosphates have terminal groups such as OH^- (12). These materials are usually considered tetrahedral–tetrahedral frameworks. There are also a number of vanadium phosphates with penta coordinate vanadium cations. In general, vanadium cations are interrupted due to certain structure features such as the presence of vanadyl bonds (V=O) (13).

We have been interested for some time in the synthesis and characterization of novel framework structures and have discovered a number of new interesting phases including some zinc (or vanadium) phosphates (14–16). Since cobalt can reside in a variety of polyhedral environments, it is a very useful candidate for constructing novel framework structures. The redox properties of cobalt make cobalt sites in open framework structures potentially useful for catalytic applications (17, 18). The magnetic properties of cobalt and

0022-4596/97 $25.00

their sensitivity to the coordination environment also provide a stimulus for their studies (19).

In this paper, we report a new sodium cobalt phosphate with a three-dimensional framework structure built from Co^{2+} in a trigonal bipyramidal environment. The framework belongs to the uninterrupted tetrahedral–penta-coordinate (trigonal bipyramidal in this case) type discussed above. The novel framework structure consists of one-dimensional channels where charge-balancing sodium cations are located. The Co–O–Co linkages lead to a cluster of four Co^{2+} ions which are likely to be responsible for the low-temperature antiferromagnetic ordering.

EXPERIMENTAL

Synthesis

$CoCO_3 \cdot xH_2O$ (0.56 g) was mixed with 8.64 g of distilled water. Carbon dioxide evolved when 1.21 g of 85% H_3PO_4 was slowly added to the above mixture. With stirring, 1.13 g of $(CH_3)_2NH$ (40 wt% solution in water) and 2.05 g of 6 *M* NaOH solution were added. The color of the gel changed from pink to blue. The mixture was then heated at 180°C for 3 days in a Teflon-coated steel autoclave. The product was recovered by filtration and washed with deionized water. Translucent dark red needle-like crystals were obtained from a mixture which also had about one half of pale pink plate-like crystals. The two different phases can be easily separated since crystals of the same phase grew into star-like clusters. They were identified as two different polymorphs of $NaCoPO_4$ by single crystal X-ray diffraction studies. The dark red phase consists of Co^{2+} in the trigonal bipyramidal coordination whereas the pink crystal (20) consists of octahedral Co^{2+} cations. The structure and magnetic properties of the dark red phase are reported below.

Magnetic Susceptibility

Susceptibility measurements on a polycrystalline sample were carried out using a Quantum Design MPMS-5S Magnetic Properties Measuring System with a sample weight of 13.3 mg. The measurements of the field dependence were carried out at temperatures of 1.7 K and 5 K. The measurements of the temperature dependence were done from 1.7 K to 300 K in an applied field of 250 G for the sample cooled in zero field and 250 G field, respectively.

Single Crystal Structure Determination

One needle-like crystal of the dark red $NaCoPO_4$ was mounted on a thin glass fiber with 5-min epoxy glue and mounted on a Siemens Smart CCD diffractometer equipped with a normal focus, 2.4 KW sealed tube X-ray source (Mo$K\alpha$ radiation, $\lambda = 0.71073$ Å) operating at 50 kV and 40 mA. About 1.3 hemisphere of intensity data were collected in 1321 frames with ω scans (width of 0.30 and exposure time of 30 s per frame). Unit cell dimensions were determined by a least-squares fit of 3389 reflections with $I > 10\sigma(I)$ and $10^\circ < 2\theta < 56^\circ$. The empirical absorption correction was based on the equivalent reflections. Other effects such as absorption by the glass fiber were simultaneously corrected. The structure was solved by Patterson methods followed by difference Fourier methods. All calculations were performed using SHELXTL running on a Silicon Graphics Indy 5000. Final full-matrix refinements were against F^2 and included secondary extinction correction and anisotropic thermal parameters for all atoms. Parameter shifts in the final least-squares cycle were smaller than 0.03σ. The crystallographic results are summarized in Table 1 while the atomic coordinates, selected bond distances, and angles are listed in Tables 2 and 3, respectively.

RESULTS AND DISCUSSION

The asymmetric unit contains two formula units of $NaCoPO_4$. Both crystallographically unique Co^{2+} ions are five-coordinate and adopt trigonal bipyramidal configurations (Fig. 1). As shown in Table 2, with the exception of O6, all oxygen atoms are bonded to at least one of two unique sodium cations. However, in describing the framework topology below, the coordinations between framework oxygen atoms and extra-framework sodium cations are not included. Of eight unique oxygen atoms, two (O1 and O6) are trigonally connected to two Co^{2+} ions and one P^{5+} ion

TABLE 1
Summary of Crystal Data and Refinement Results

Structural formula	$NaCoPO_4$
Formula weight	176.89
Color and habit	dark red needle
Crystal size (mm^3)	$0.30 \times 0.13 \times 0.083$
a(Å)	5.7856(1)
b(Å)	11.0954(2)
c(Å)	9.9228(3)
β(°)	92.668(2)
V(Å^3)	636.29(2)
Z	8
Space group	$P2_1/c$ (No. 14)
ρ_{calc} (g/cm^3)	3.693
λ(Mo$K\alpha$) (Å)	0.71073
μ(Mo$K\alpha$) (mm^{-1})	5.867
Maximum 2θ	56.54°
Observed data $I > 2\sigma(I)$	1471
Parameters	128
$R(F)^a$	2.07%
$R_w(F^2)^b$	5.53%
GOF	1.19

[a] $R(F) = \sum||F_o| - |F_c||/\sum|F_o|$ with $F_o > 4.0\sigma(F)$.
[b] $R(F^2) = [\sum[w(F_o^2 - F_c^2)^2]/\sum[w(F_o^2)^2]]^{1/2}$ with $F_o > 4.0\sigma(F)$. $w = 1/[\sigma^2(F_o^2) + (0.0216P)^2 + 1.0690P]$ where $P = (F_o^2 + 2F_c^2)/3$.

TABLE 2
Atomic Coordinates ($\times 10^4$) and Equivalent Isotropic Displacement Parameters ($Å^2 \times 10^3$)

	x	y	z	$U_{(eq)}$[a]
Co(1)	− 1104(1)	11037(1)	− 7328(1)	8(1)
Co(2)	− 3473(1)	8788(1)	− 4984(1)	8(1)
P(1)	− 3764(1)	6152(1)	− 6703(1)	6(1)
P(2)	1240(1)	8627(1)	− 5873(1)	6(1)
Na(1)	− 1245(2)	6308(1)	− 3782(1)	20(1)
Na(2)	− 6204(2)	6523(1)	− 3693(1)	18(1)
O(1)	− 952(3)	9389(1)	− 6253(2)	9(1)
O(2)	− 4065(3)	10334(2)	− 8277(2)	10(1)
O(3)	1549(3)	10365(2)	− 8491(2)	11(1)
O(4)	1520(3)	7711(2)	− 6985(2)	11(1)
O(5)	− 848(3)	11964(2)	− 5502(2)	12(1)
O(6)	− 6582(3)	9424(1)	− 5763(2)	9(1)
O(7)	− 3842(3)	7022(2)	− 5503(2)	10(1)
O(8)	− 3654(3)	8147(2)	− 3046(2)	11(1)

[a] $U_{(eq)}$ is defined as one third of the trace of the orthogonalized U_{ij} tensor.

TABLE 3
Selected Bond Lengths (Å) and Angles (°)

Co(1)–O(4)	1.989(2)	Co(1)–O(2)	2.069(2)
Co(1)–O(5)	2.083(2)	Co(1)–O(3)	2.100(2)
Co(1)–O(1)	2.117(2)	Co(2)–O(7)	2.034(2)
Co(2)–O(6)	2.051(2)	Co(2)–O(8)	2.057(2)
Co(2)–O(1)	2.080(2)	Co(2)–O(6)	2.118(2)
P(1)–O(7)	1.535(2)	P(1)–O(8)	1.546(2)
P(1)–O(2)	1.549(2)	P(1)–O(3)	1.556(2)
P(2)–O(4)	1.515(2)	P(2)–O(6)	1.539(2)
P(2)–O(5)	1.540(2)	P(2)–O(1)	1.555(2)
Na(1)–O(7)	2.359(2)	Na(1)–O(5)	2.393(2)
Na(1)–O(3)	2.469(2)	Na(1)–O(2)	2.512(2)
Na(1)–O(4)	2.580(2)	Na(1)–O(8)	2.595(2)
Na(1)–O(1)	2.624(2)	Na(1)–O(3)	2.899(2)
Na(2)–O(4)	2.353(2)	Na(2)–O(7)	2.373(2)
Na(2)–O(4)	2.353(2)	Na(2)–O(7)	2.373(2)
Na(2)–O(8)	2.397(2)	Na(2)–O(2)	2.430(2)
Na(2)–O(3)	2.478(2)	Na(2)–O(5)	2.497(2)
O(4)–Co(1)–O(2)	96.39(7)	O(4)–Co(1)–O(5)	80.75(7)
O(2)–Co(1)–O(5)	127.30(7)	O(4)–Co(1)–O(3)	102.92(7)
O(2)–Co(1)–O(3)	103.10(7)	O(5)–Co(1)–O(3)	129.02(7)
O(4)–Co(1)–O(1)	168.74(7)	O(2)–Co(1)–O(1)	85.30(6)
O(5)–Co(1)–O(1)	89.35(6)	O(3)–Co(1)–O(1)	87.47(6)
O(7)–Co(2)–O(6)	98.98(6)	O(7)–Co(2)–O(8)	83.98(7)
O(6)–Co(2)–O(8)	112.93(7)	O(7)–Co(2)–O(1)	102.90(6)
O(6)–Co(2)–O(1)	106.78(7)	O(8)–Co(2)–O(1)	138.08(7)
O(7)–Co(2)–O(6)	172.12(6)	O(6)–Co(2)–O(6)	78.93(7)
O(8)–Co(2)–O(6)	89.83(6)	O(1)–Co(2)–O(6)	84.96(6)
O(7)–P(1)–O(8)	110.86(9)	O(7)–P(1)–O(2)	108.97(9)
O(8)–P(1)–O(2)	110.48(9)	O(7)–P(1)–O(3)	108.08(9)
O(8)–P(1)–O(3)	108.82(9)	O(2)–P(1)–O(3)	109.59(9)
O(4)–P(2)–O(6)	108.79(9)	O(4)–P(2)–O(5)	112.63(10)
O(6)–P(2)–O(5)	109.63(9)	O(4)–P(2)–O(1)	107.57(9)
O(6)–P(2)–O(1)	11.13(9)	O(5)–P(2)–O(1)	107.10(9)

while the other oxygen atoms are connected between one Co^{2+} ion and one P^{5+} ion (Fig. 2). These two trigonally coordinated oxygen atoms are only associated with P2 tetrahedra and are not directly connected to P1. Thus P1 tetrahedra are connected to only four other cobalt bipyramids through oxygen bridges while P2 tetrahedra are connected to six other cobalt bipyramids (Fig. 1).

One notable difference between Co1 and Co2 is that a pair of Co2 bipyramids share an edge and is located on the inversion center while Co1 bipyramids are separated by

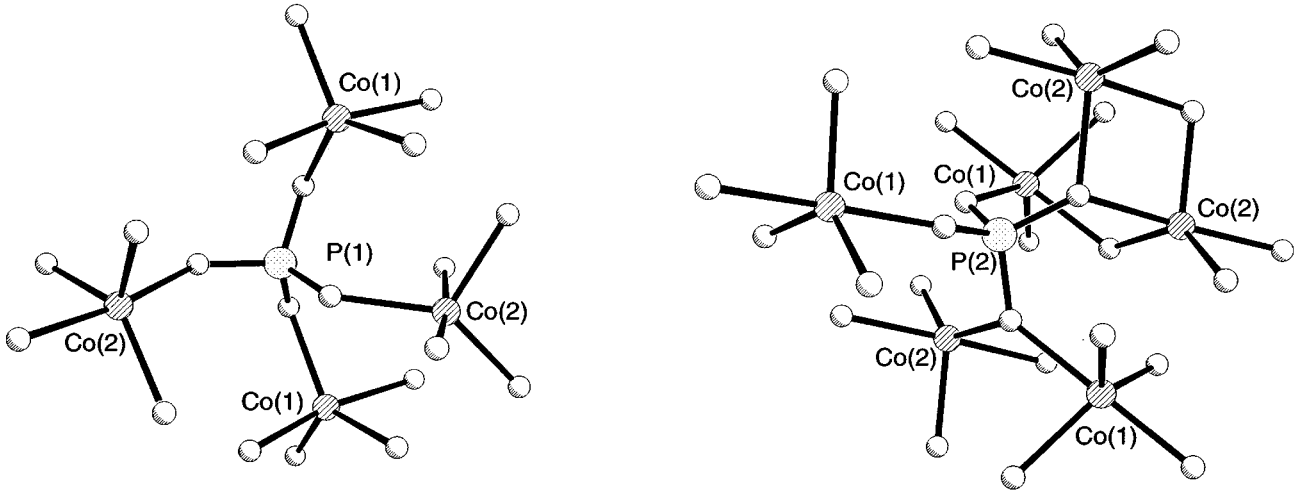

FIG. 1. Coordination environments for the two unique phosphorous tetrahedra (P1 and P2). The P2 tetrahedron is connected to six cobalt polyhedra through oxygen bridges.

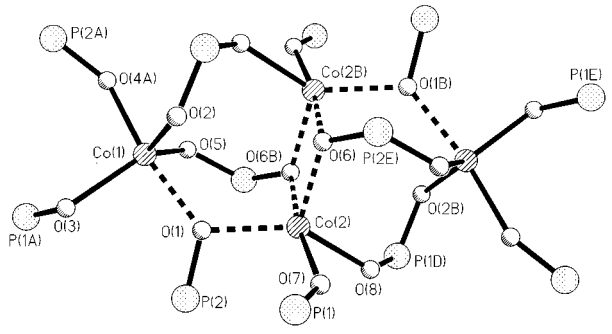

FIG. 2. The Co–O–Co linkage joins four Co^{2+} ions into a tetramer as illustrated with dashed bonds. Not all atoms are labelled since the cluster shown here displays the symmetry of inversion center. Atoms with labels containing "A", "B", ..., "E" are symmetry-generated.

Co2, P1, and P2 oxygen polyhedra. Each Co2 bipyramid in the pair is corner-shared to one Co1 bipyramid, thus forming a cluster of four Co^{2+} ions with O1 and O6 as bridges (Fig. 2). It is likely that the antiferromagnetic ordering described later in this paper occurs in such a cluster.

The three-dimensional connectivity between cobalt and phosphorous polyhedra is rather complex. To simplify the analysis, either Co1 or Co2 can be regarded as an extra-framework species just like sodium cations. Such an analysis also helps one understand the framework stoichiometry from its connectivity. As described below, a three-dimensional framework still exists if either Co1 or Co2 cations are considered as extra-framework species filling the cavities.

If Co1 cations are treated as extra-framework species, the edge-sharing Co2 dimer behaves like eight-coordinate polyhedral center and is connected to eight phosphorous tetrahedra. The phosphate group is effectively a bidentate linking two Co2 dimers. Each Co2 dimer is connected to four other Co2 dimers through four P1 tetrahedral groups (Fig. 3) and to two more Co2 dimers through two pairs of P2 tetrahedral double bridges (Fig. 3). Thus, a ratio of 1/2 can be derived for Co2/(P1 + P2) from this type of connectivity.

As shown in Fig. 3b, P2 tetrahedra connect Co2 dimers into chains along the crystallographic *a*-axis and these chains are cross-linked by P1 tetrahedra in two other mutually perpendicular directions into a three-dimensional framework. Thus a three-dimensional network formed from P1, P2, and Co2 polyhedra can be regarded as cross-linked chains. The filling of cavities by Co1 cations is shown in Fig. 3a.

Another way to view the framework connectivity is to consider Co2 cations as cavity-filling extra-framework species. In this view, the framework is built from identical layers and in projection these layers are eclipsed. Each layer consists of 4-rings and 8-rings formed from P2 tetrahedra and Co1 bipyramids (Fig. 4a) and the layer can be classified as a distorted (4.8^2) net commonly found in zeolite frameworks (21). The layers are interconnected by P1 tetrahedra. Each P1 tetrahedron joins two Co1 polyhedra which are separated by a distance corresponding to the length of the *a*-axis. Thus the framework consists of 2-D nets formed from Co1 and P2 polyhedra and 1-D zigzag chains (perpendicular to the 2-D net) formed from Co1 and P1 polyhedra. This gives a ratio of 1/2 for Co1/(P1 + P2).

The framework consists of channels propagating along the *a*-axis. Within each channel, there are two columns of sodium cations. Two crystallographically unique Na^+ ions do not form two separate columns (Fig. 4b). Instead they alternate in the same column.

The temperature dependence of magnetic susceptibility data for the sample cooled in zero field is shown in Fig. 5.

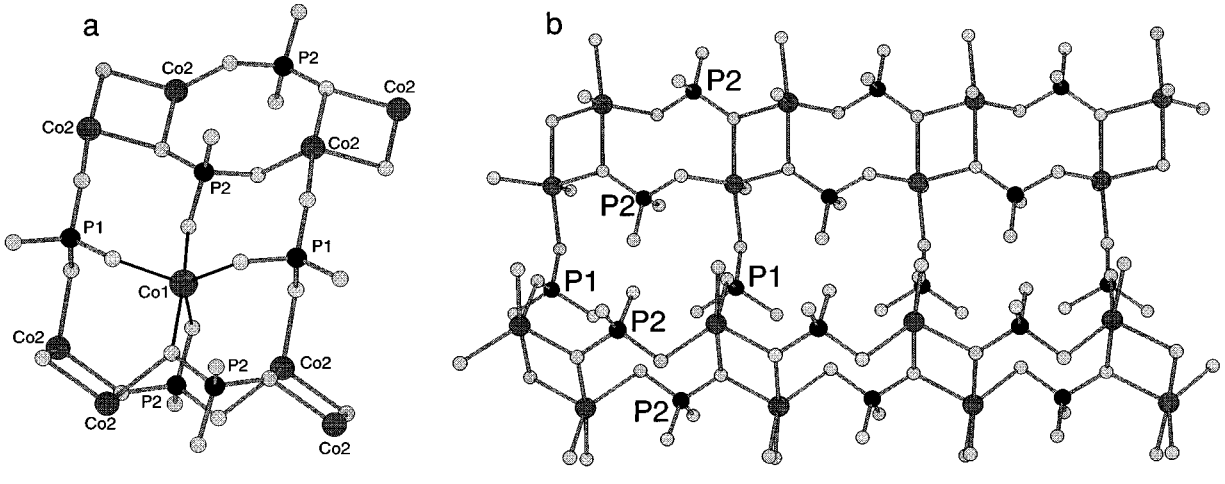

FIG. 3. (a) An illustration of one of Co1 cations located in the cavities of P1–Co2–P2 oxygen framework. (b) Two chains along the *a*-axis (from left to right) formed by connecting Co2 dimers with P2 tetrahedra. The interchain connection is through P1 tetrahedra.

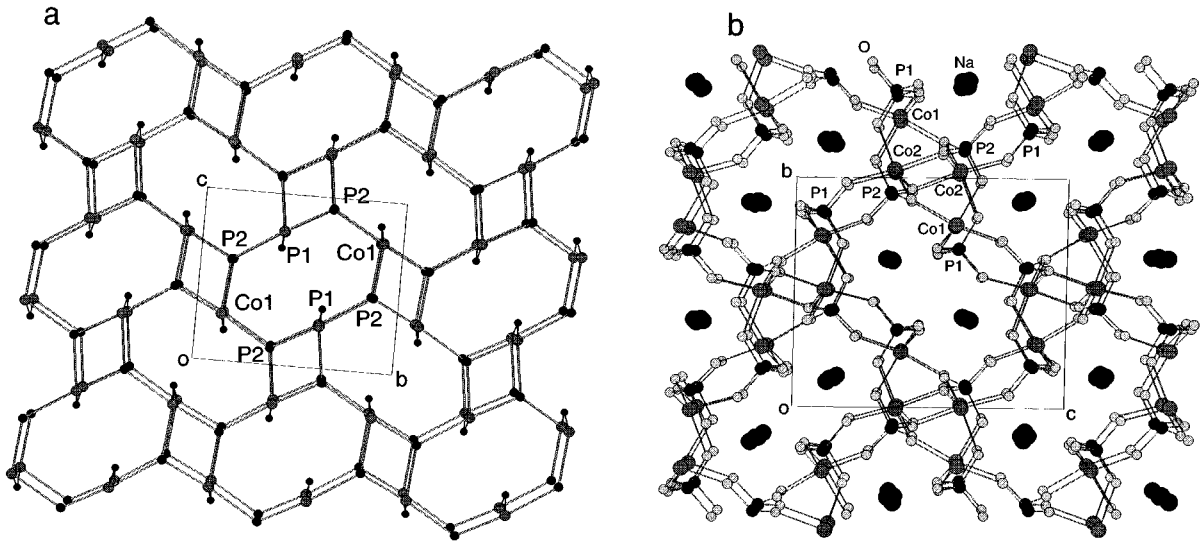

FIG. 4. (a) Polyhedral-atom connectivity diagram for P1–Co1–P2 framework with bridging oxygen atoms omitted for clarity. The three-connected 2-D nets (the 4.8^2 net) are joined with P1 tetrahedra and are eclipsed in projection. (b) The framework structure viewed along the channel direction (the shortest crystallographic axis, *a*-axis) showing sodium ions occupying positions inside channels.

The temperature dependence for the sample cooled in 250 G field shows the same behavior. The field dependence of magnetization is shown in Fig. 6. Since there is very little difference between 1.7 and 5 K data, only the field dependence at 5.0 K is shown. The susceptibility data exhibit Curie–Weiss paramagnetism down to a temperature of 15 K at which the sample turns antiferromagnetic. Thus the maximum in the magnetic susceptibility is observed at 15 K. A very small increase of χ at temperatures below 4 K is likely due to the presence of a small amount of paramagnetic impurities. A linear curve fit to the Curie–Weiss law with data between 50 and 300 K gives $C = 2.93$ emu K/mol, $\theta = -24.5$ K. This gives a magnetic moment of 4.84 μ_B, which falls within the range typically observed for trigonal bipyramidal Co^{2+} ions (4.26–5.03 μ_B) (22). For three unpaired electrons, the g value is calculated to be 2.50. The $M(H)$ behavior shows a straight line which is typical of paramagnetic or antiferromagnetic behavior.

It is of interest to compare the $NaCoPO_4$ phase (the red phase) reported here with two other polymorphs of $NaCoPO_4$ (the blue phase (23) and the pink phase (20)). The three phases not only differ in the coordination geometry of cobalt cations (tetrahedral for the blue phase, octahedral for the pink phase), but also differ in the connectivity of phosphate groups to cobalt polyhedra. The three different polymorphs have very different space group symmetry (blue,

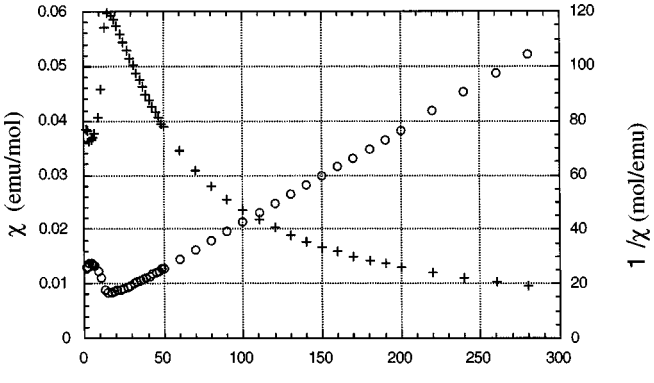

FIG. 5. Molar susceptibility and inverse molar susceptibility plotted as a function of temperature over the 1.7–300 K region.

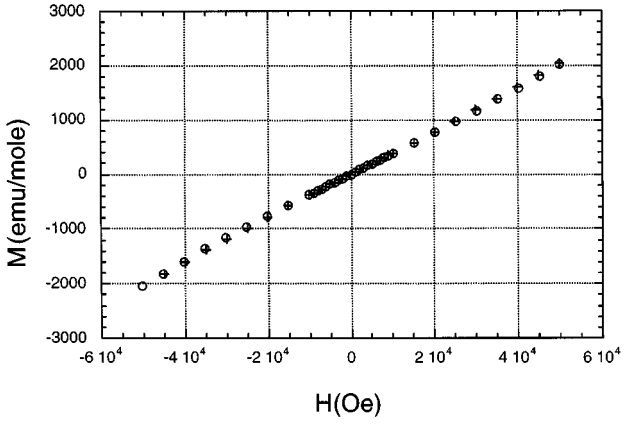

FIG. 6. Magnetization (M) as function of applied magnetic field (H) at $T = 5.0$ K. The open circles are data collected on decreasing field and the plus symbols are data collected on increasing field.

$P6_1$; red, $P2_1/c$; pink, *Pnma*) and the framework connectivity, however, somewhat surprisingly, a ratio of 1 between polyhedral centers (Co/P) is maintained in all three polymorphs.

In terms of connectivity to other parts of the structure, the trigonal bipyramidal coordination of Co^{2+} cations lies between the tetrahedral and octahedral phases and the same is true for the phosphate groups too. While each P^{5+} cation is connected to four Co^{2+} tetrahedra in the blue phase and six Co^{2+} octahedra in the pink phase through the oxygen bridges, each of the half of the P^{5+} tetrahedra (P1) in the red phase is connected to four Co^{2+} polyhedra while each of the other half P^{5+} tetrahedra (P2) is connected to six Co^{2+} polyhedra. The red phase ($d = 3.693\ g\,cm^{-3}$) is slightly less dense than the pink phase ($d = 3.858\ g\,cm^{-3}$). This indicates that the higher coordination number leads to a denser structure. This is further supported by the fact that the third polymorph (the blue tetrahedral phase) has the lowest density ($d = 3.274\ g\,cm^{-}3$). Since a coordination of 4 is the minimum needed to form a three-dimensional framework, the trend in the density of three cobalt polymorphs is consistent with the observation that the majority of microporous structures are tetrahedral frameworks.

Synthetically, we have observed that the red phase can co-crystallize with either the blue phase or the pink phase. However, a mixture of blue and pink phases has not been observed. Of the three polymorphs of $NaCoPO_4$ salts which contain tetrahedral, trigonal bipyramidal, and octahedral cobalt cations, the red phase described here has the most complex framework. While we have found that both blue and pink phases are members of two different families of isotypic structures (19, 24), so far no other structure has been known to have the same framework connectivity as the red phase described here.

The antiferromagnetic ordering at temperatures of 13 K for the pink phase and of 15 K for the red phase agrees with the structural features found in the two polymorphs with infinite Co–O–Co chains in the pink phase and Co–O–Co clusters in the red phase. Since there is no Co–O–Co linkage in the blue phase it is paramagnetic down to a temperature of 3 K. The red phase and the pink phase show different $M(H)$ behaviors, however. The $M(H)$ curve for the red phase is linear throughout the range measured (up to 5×10^4 G) whereas the pink phase has a magnetic phase transition at a critical field of 4×10^4 G. This can be attributed to the difference in Co–O–Co linkages.

ACKNOWLEDGMENTS

This research was supported in part by the National Science Foundation under Grant DMR 95-20971. We thank Dr. Sarah H. Tolbert for assistance in susceptibility measurements.

REFERENCES

1. D. W. Breck, "Zeolite Molecular Sieves, Structure Chemistry, and Use." Wiley, New York, 1974.
2. P. B. Moore and J. Shen, *Nature* **306,** 356–358 (1983).
3. T. M. Nenoff, W. T. A. Harrison, and G. D. Stucky, *Chem. Mater.* **6,** 525–530 (1994).
4. T. E. Gier, X. Bu, S.-L. Wang, and G. D. Stucky, *J. Am. Chem. Soc.* **118,** 3039 (1996).
5. W. T. A. Harrison, T. E. Gier, and G. D. Stucky, *Angew. Chem. Int. Ed. Engl.* **32,** 724 (1993).
6. M. Mathew, L. W. Schroeder, and T. H. Jordan, *Acta Crystallogr. B* **33,** 1812–1816 (1977).
7. W. M. Reiff, M. J. Kwiecien, R. J. B. Jakeman, A. K. Cheetham, and C. C. Torardi, *J. Solid State Chem.* **107,** 401–412 (1993).
8. A. Modaressi, A. Courtois, R. Gerardin, B. Malaman, and C. Gleitzr, *J. Solid State Chem.* **47,** 245–255 (1983).
9. J. S. Stephens and C. Calvo, *Can. J. Chem.* **45,** 2303 (1967).
10. M. Bouchdoug, A. Courtois, R. Gerardin, J. Steinmetz, and C. Gleitzer, *J. Solid State Chem.* **42,** 149–157 (1982).
11. I. Tordjman, J. C. Guitel, A. Durif, M. T. Averbuch, and R. Masse, *Mat. Res. Bull.* **13,** 983–988 (1978).
12. J. A. Martens and P. A. Jacobs, *in* "Advanced Zeolite Science and Applications, Studies in Surface Science and Catalysis" (J. C. Jansen, M. Stocker, H. G. Karge, and J. Weitkamp, Eds.), Vol. 85. Elsevier, Amsterdam, 1994.
13. M. I. Khan, L. M. Meyer, R. C. Haushalter, A. L. Schweitzer, J. Zubieta, and J. L. Dye, *Chem. Mater.* **8,** 43–53 (1996).
14. X. Bu, P. Feng, and G. D. Stucky, *J. Chem. Soc., Chem. Comm.* 1337 (1995).
15. P. Feng, X. Bu, and G. D. Stucky, *Angew. Chem., Int. Ed. Engl.* **34,** 1745 (1995).
16. X. Bu, P. Feng, and G. D. Stucky, *J. Solid State Chem.* **125,** 243–248 (1996).
17. S. S. Lin and H. S. Weng, *Appl. Catal. A* **105,** 289 (1993).
18. J. Dakka and R. A. Sheldon, Netherlands Pat. 9,200,968 (1992).
19. R. L. Carlin, "Magnetochemistry," Springer-Verlag, Berlin/New York, 1986.
20. P. Feng, X. Bu, and G. D. Stucky, submitted for publication.
21. H. V. Koningsveld, *in* "Introduction to Zeolite Science and Practice, Studies in Surface Science and Catalysis" (H. Bekkum, E. M. Flanigen, and J. C. Jansen, Eds.), Vol. 58. Elsevier, Amsterdam, 1991.
22. L. Banci, A. Bencini, C. Benelli, D. Gatteschi, and C. Zanchini, *Struct. Bond.* **52,** 37 (1982).
23. P. Feng, X. Bu, S. H. Tolbert, and G. D. Stucky, *J. Am. Chem. Soc.*, in press.
24. O. Muller and R. Roy, "The Major Ternary Structural Families," Springer-Verlag, Berlin/New York, 1974.